

Selective linewidth control in a micro-resonator with a resonant interferometric coupler

Paula L. Pagano,^{1,2} Massimo Borghi,^{3,*} Federica Moroni,³ Alice Viola,³
Francesco Malaspina,³ Marco Liscidini,³ Daniele Bajoni,² and Matteo Galli³

¹*Centro de Investigaciones Ópticas, CONICET-CICBA-UNLP,
Camino Centenario y 505 s/n , 1897 Gonnet, Argentina.*

²*Dipartimento di Ingegneria Industriale e dell'Informazione,
Università di Pavia, Via Ferrata 5, 27100 Pavia, Italy.*

³*Dipartimento di Fisica, Università di Pavia, Via Bassi 6, 27100 Pavia, Italy.*

(Dated: April 25, 2024)

Optical microresonators are characterized by a comb of resonances that preserve similar characteristics over a broad spectral interval. However, for many applications it is beneficial to selectively control of the quality factor (Q) of one or only some resonances.

In this work we propose and experimentally validate the use of a resonant interferometric coupler to selectively change the Q-factor of a target resonance in an integrated silicon nitride microresonator. We show that its Q-factor can be continuously tuned from 6.5×10^4 to 3×10^6 , leaving the untargeted resonances unperturbed. Our design can be scaled to independently control several resonances.

I. INTRODUCTION

Integrated optical microresonators are versatile devices which find use in several applications, such as spectral filters, switches [1–4], delay lines [5, 6], sensors [7, 8], modulators [9, 10] and light sources [11]. Microresonators are typically characterized by a comb of resonances that preserve similar characteristics, such as the quality factor or the extinction rate, over a broad spectral interval. This feature is harnessed to generate broadband frequency combs [12], soliton pulses [13], or photon pairs in high dimensional entangled states [14]. However, some applications may require the selective and dynamic control of the quality factor (Q) of only some of the resonances. Examples include Q-switched lasers [15, 16], single frequency lasers [17], tunable modulators [18], tunable delay lines [19], optical memories [20], pseudo-random binary sequence generators [21] and photon pair sources with tailored spectral correlations [22] or high heralding efficiency [23, 24]. Several approaches have been investigated to control the Q-factor [17, 18, 20, 24–30], and some of them are wavelength selective [17, 20, 24–26, 29, 30]. For example, a strong control pulse has been used to induce Raman scattering in silicon on a target resonance [25]. However, this operation can be done efficiently only at the maximum of the Raman gain of the material, and demands strict fabrication tolerances [25, 26]. The Q-factor can also be tuned by varying the phase shift in an unbalanced interferometer forming the coupling region of a microresonator [18, 28]. Alternatively, the Q-factor of a single resonance can be changed due to the strong coupling with another resonator [17, 20, 29, 30]. or by a combination of the previous strategies [24]. In this work, we propose and experimentally demonstrate the selective control of the Q-factor of a single resonance

in a microresonator by using a resonant interferometric coupler. A Main resonator is coupled twice to a bus waveguide to form an unbalanced Mach-Zehnder interferometer (MZI). Then, we introduce an auxiliary resonator (Aux) in one of the arms to impart a wavelength-selective phase. This changes the interference within the MZI and thus the effective coupling coefficient with the input waveguide. The article is structured as follows: in Sec.II we describe the working principle of the device and explore different configurations which allows us to selectively change the Q-factor of a target resonance. The device is then fabricated on a silicon nitride chip, and its experimental characterization is reported in Sec.III. Here we show that the Q-factor of the target resonance can be continuously changed from 6.5×10^4 to 3×10^6 with minimal perturbation of the adjacent ones.

II. WORKING PRINCIPLE OF THE DEVICE

The proposed structure is sketched in Fig.1. A main ring resonator (Main) of radius R is coupled twice to a bus-waveguide at points A and B, with coupling coefficients κ_A and κ_B respectively, to form an interferometric coupler [18]. An auxiliary resonator of radius R_{Aux} is also coupled to the bus waveguide at point C. The highlighted area in Fig.1 can be seen as a Mach-Zehnder interferometer (MZI), with a first arm of length πR along the Main ring, and a second arm of length l along the bus-waveguide.

The effective coupling of the Main ring resonator to the bus waveguide depends on the phase difference between the two MZI arms [18, 28, 31]. Such a difference is given by two distinct contributions: the imbalance in the optical length of the two interferometer arms, and the transmission of the Aux ring. The former contribution acts at all frequencies, the latter is relevant only when its frequency is within the spectral width of an Aux ring res-

* corresponding author: massimo.borghi@unipv.it

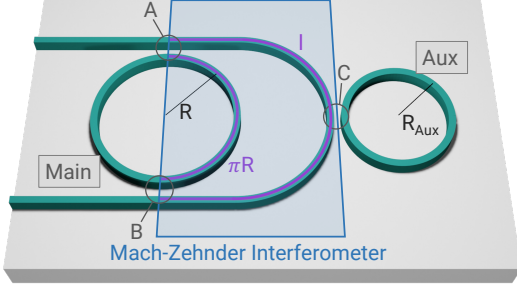


FIG. 1. Sketch of the proposed device. Waveguides are shown in green, while the lower cladding region is shown in gray.

onance. Thus, one has two sets of resonances that can be controlled independently: those that belong only to the Main ring and those that are shared with the Aux. For instance, by choosing incommensurate values for R and R_{Aux} , it is possible to selectively control one single resonance. Using a microheater, one can adjust the refractive index of the bus waveguide to set the desired coupling for all the other Main resonances. An additional microheater can act on the Aux to align one of its resonances to the target Main ring resonance.

With reference to Fig.1, the device transmission T at the output port can be written as

$$T = \left| \frac{e^{i\tilde{\phi}_{Main}} \sigma_A \sigma_B \delta_{MZI} - \kappa_A \kappa_B - \delta_{MZI} e^{i2\tilde{\phi}_{Main}}}{1 - [\sigma_A \sigma_B - \kappa_A \kappa_B \delta_{MZI}] e^{i2\tilde{\phi}_{Main}}} \right|^2, \quad (1)$$

where σ_j and κ_j are the self- and cross-coupling coefficients at point $j \in \{A, B, C\}$, $\tilde{\phi}_{Main} = \tilde{\beta}\pi R$ and $\tilde{\beta} = \beta + i\frac{\alpha}{2}$ is the complex wavevector, which accounts for both propagation (β) and linear attenuation (α). Finally,

$$\delta_{MZI} = t_{Aux} e^{i\tilde{\beta}(l - \pi R)} \quad (2)$$

describes the attenuation and phase difference acquired between the two arms of the MZI, and

$$t_{Aux} = \frac{\sigma_C - e^{i\tilde{\phi}_{Aux}}}{1 - \sigma_C e^{i\tilde{\phi}_{Aux}}}, \quad (3)$$

is the transmission amplitude of the Aux resonator, with $\tilde{\phi}_{Aux} = \tilde{\beta}2\pi R_{Aux}$.

Unsurprisingly, Eq.(1) is equivalent to the transmission of a resonator in the all-pass filter configuration in which the effective coupling coefficient κ_{eff}^2 with the input waveguide is given by

$$|\kappa_{eff}|^2 = |\kappa_A \sigma_B + \kappa_B \sigma_A \delta_{MZI}|^2, \quad (4)$$

which is the expression for the cross port transmission of the MZI, where $\Delta\phi_{MZI} = \beta(l - \pi R) + \arg[t_{Aux}]$.

We now consider the special case in which $l = 3\pi R$. Thus, for all of the resonances that are spectrally far from

those of the Aux (for which $|\delta_{MZI}| \sim 1$ and $\arg[t_{Aux}] \sim 0$) we have that the phase difference in the MZI is a multiple of 2π , and the interference is constructive at the cross port of the MZI. In this situation, when $\kappa_A = \kappa_B$, the effective coupling is maximum and equal to $|\kappa_{eff}|^2 = 4\kappa_A^2 \sigma_A^2$. Changing $\Delta\phi_{MZI}$ through a micro-heater placed in the long arm of the MZI modifies κ_{eff}^2 for all the resonances. However, if the Aux resonator is used to change the interference condition at the MZI, the effective coupling is modified only in the neighborhood of the Aux resonances. It is then possible to vary the effective coupling of the Main ring from a completely uncoupled condition, when interference is destructive, to an over-coupled condition, when the interference is constructive.

We further set $R_{Aux} = \frac{3}{4}R$ so that only one resonance out of four in the Main ring will overlap with one of the Aux, leaving the other resonances largely detuned from any Aux resonance. We consider the case in which the Aux is massively over-coupled, so that most of the light is efficiently coupled into it and back to the MZI before it is lost by scattering.

In Fig.2 we show the spectral transmission T , the cosine of $\Delta\phi_{MZI}$, and the intensity enhancement (IE) in the Main ring for different MZI and Aux configurations. The spectral position of the Aux resonances can be clearly seen as sharp variations in the otherwise smooth sinusoidal oscillations of $\cos(\Delta\phi_{MZI})$. In Fig.2(a), $\beta(2\pi R) = 2m\pi$, so κ_{eff}^2 is maximized and the Main ring is maximally over-coupled. The Aux is detuned from all the Main resonances, which are then unperturbed and have the same value of the IE. In Fig.2(b) we show the response of the structure with an Aux resonance matching a target Main resonance at the wavelength λ_0 , which is highlighted in yellow. The Main ring becomes completely uncoupled at λ_0 due to the additional phase imparted by the Aux resonator, which causes $\Delta\phi_{MZI}(\omega_0) = \pi$ and sets the MZI to a completely destructive interference at its cross port.

Figure 2(c) shows the effect of a slight detuning of the MZI from the configuration shown in Fig.2(b). Here $\Delta\phi_{MZI} > 0$ for all the resonances, and the π phase shift given by the Aux does not uncouple the target resonance anymore because it causes $\Delta\phi > \pi$. We choose the MZI detuning such that the target resonance is brought to a critical coupling condition when it is overlapped by the Aux ($\kappa_{eff} = \kappa_{cc}$, where κ_{cc} is the coupling coefficient for which the intrinsic loss perfectly balances the coupling loss with the input waveguide), while the other ones are still over-coupled. This condition is also clearly witnessed from the large IE at the target resonance.

In the last configuration, reported in Fig.2(d), we show that reverse behavior is possible as well: a target resonance in a comb of critically coupled ones can be brought to overcoupling due to the use of the Aux resonator. The IE at the target resonance is now greatly reduced compared to the neighboring ones. In Sec.III we will show that the Aux resonator can be swept continuously across the Main resonance, thus realizing all the coupling conditions described above.

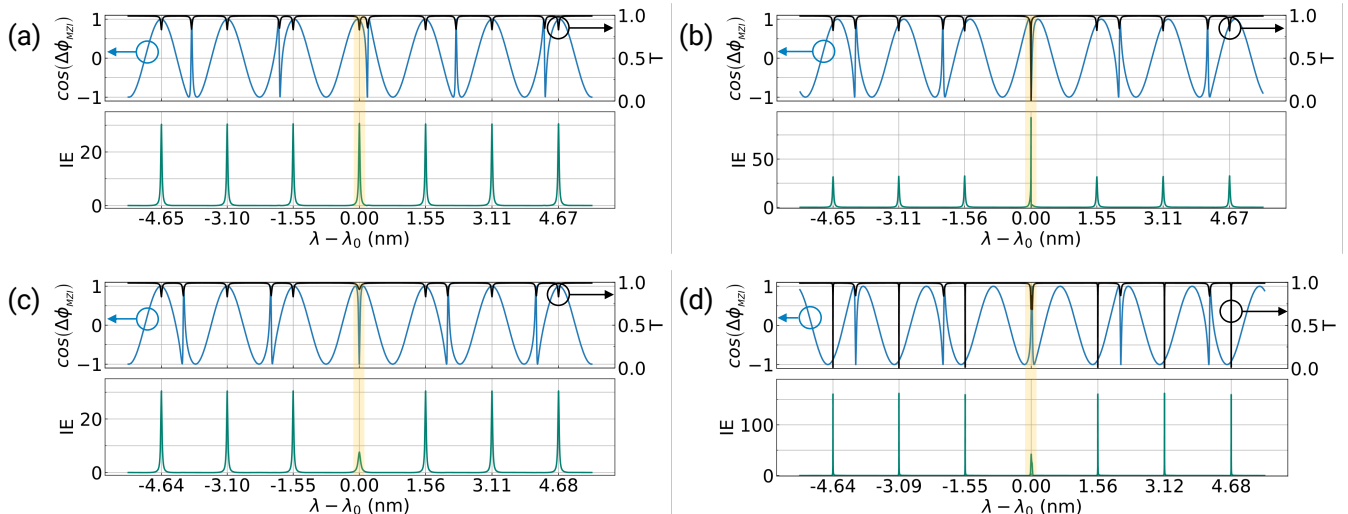


FIG. 2. Cosine of the MZI dephasing $\Delta\phi_{\text{MZI}}$ (blue), normalized transmission T (black), and intensity enhancement spectra (green) as a function of the detuning from a target resonance at wavelength λ_0 (highlighted in yellow). In this simulation, we set $\kappa_A^2 = \kappa_B^2 = 0.03$, $R = 116.6 \mu\text{m}$, $\alpha = 0.1 \text{ dB/cm}$ and $\kappa_C = 0.1$. (a) $\Delta\phi_{\text{MZI}} = 2m\pi$ and the Aux resonator is detuned from all the Main resonances. (b) Same as in (a), but the Aux resonator is tuned to match the highlighted resonance. (c) The Aux ring turns the target resonance to critical coupling when one of its resonances is tuned at λ_0 . (d) The MZI fringes are detuned to have a comb of critically coupled Main resonances, while the Aux resonator overcouples the target resonance.

III. EXPERIMENTAL RESULTS

The device described in Sec.II is fabricated on a silicon nitride photonic chip. An optical microscope image is shown in Fig.3(a). Three metallic heaters allow us to respectively change the resonance wavelength of the Main ring, of the Aux resonator, and the phase of the bus-waveguide arm $\phi_{\text{wg}} = e^{i\beta d}$ through the thermo-optic effect. The sample is mounted on a holder that is thermally stabilized, and the metallic micro-heaters are controlled by a voltage driver module. The waveguide has width of $1.75 \mu\text{m}$ and thickness of 800 nm , while the gap between the Main resonator and the bus-waveguide is $0.4 \mu\text{m}$. The setup used to probe the device transmission T is shown in Fig. 3(a). A tunable laser is coupled to a fiber polarization controller (FPC) and the polarization is controlled to match that of the TE mode of the silicon nitride waveguide. Light is coupled into and out of the chip through a fiber array of UHNA4 fibers with a coupling loss of approximately 1.7 dB/facet . Then, the output signal is detected by a powermeter and recorded in real-time by an oscilloscope.

Initially, ϕ_{MZI} is set to ensure that all the resonances of the Main resonator which are not perturbed by the Aux are critically coupled. This configuration mimics that shown in Fig.2(d). Figure 3(b) shows the device transmission when the Aux resonances are all detuned from those of the Main resonator. We can distinguish the Main from the Aux resonances from their different free spectral range (FSR), linewidth and extinction. In particular, the resonances of low extinction are those of the Aux resonator because it is heavily overcoupled. The

Main resonator has an FSR of 1.56 nm . From the resonance linewidth in the critical coupling configuration we estimated an intrinsic Q-factor of $\sim 3.2 \times 10^6$ and

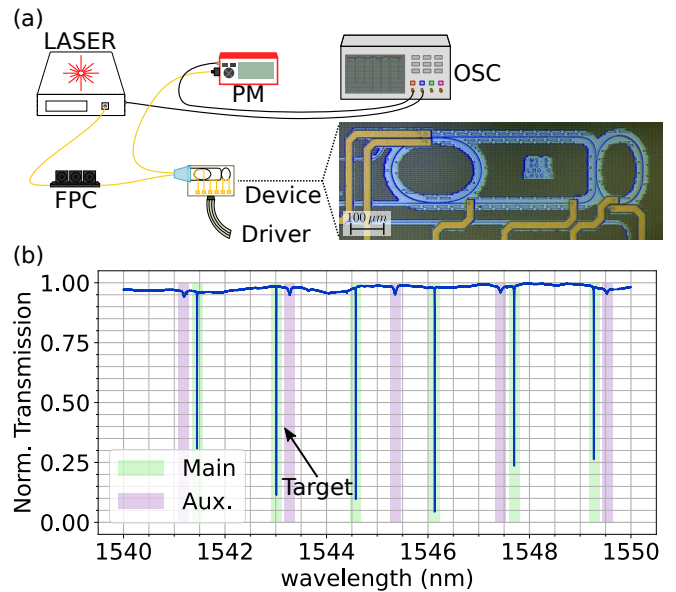


FIG. 3. (a) Sketch of the experimental setup FPC: fiber polarization controller, PM: power meter, OSC: oscilloscope. The right-inset shows an optical microscope image of the device. (b) Transmission spectra of the device. A resonance of the Main resonator is highlighted in green, while a resonance of the Aux resonator is highlighted in violet. The arrow indicates the target resonance at $\lambda_0 = 1542.97 \text{ nm}$

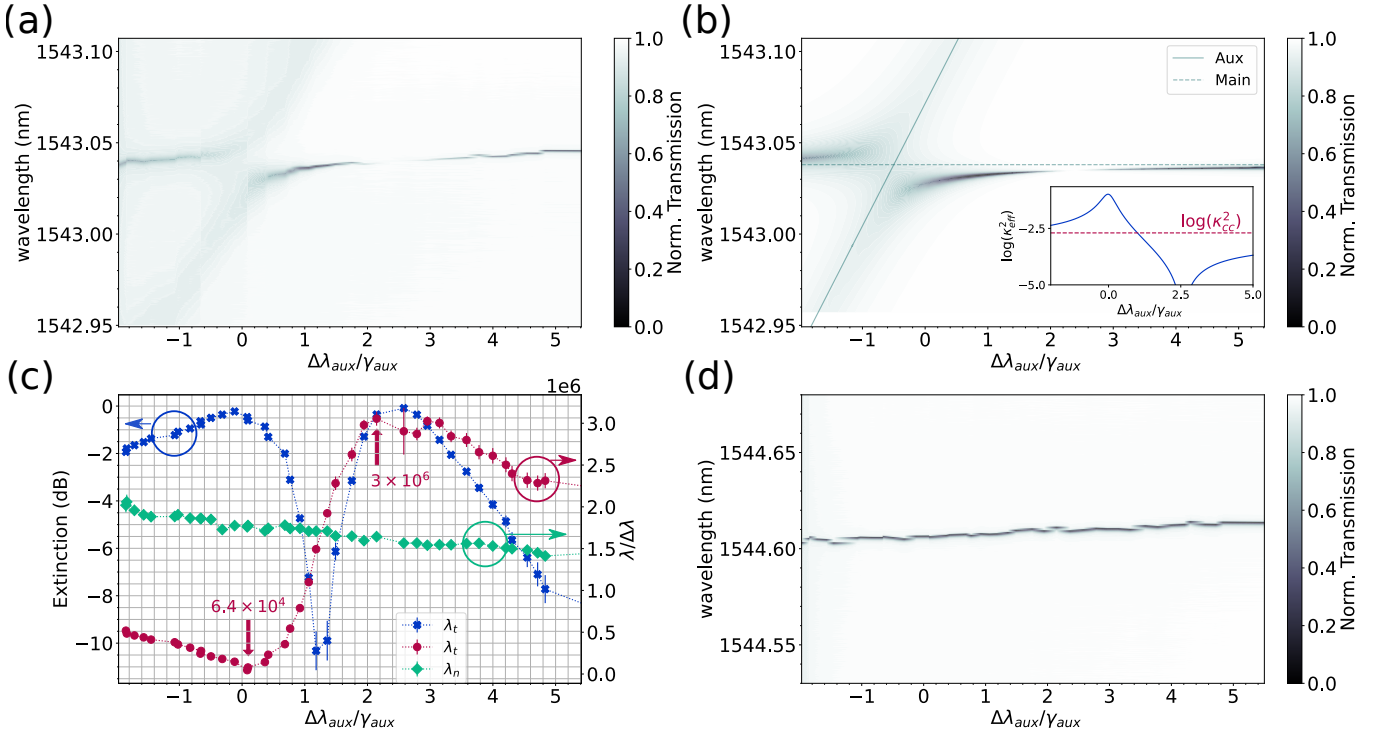


FIG. 4. (a) Stacked spectra of the target Main resonator resonance (see Fig.3(b)) for different normalized wavelength detunings of the Aux resonator $\Delta\lambda_{\text{aux}}/\gamma_{\text{aux}}$. (b) Simulation of the device transmission spectra T using Eq.(1). Inset: (logarithm) of the effective coupling coefficient κ_{eff}^2 (blue) and value of $\kappa_{\text{cc}}^2 = \kappa_{\text{cc}}^2$ at critical coupling (dashed violet line). (c) Extinction (blue) and $\lambda/\Delta\lambda$ (violet) of the target resonance λ_0 . The $\lambda/\Delta\lambda$ of an adjacent resonance at $\lambda_n \sim 1544.6$ nm is shown in green. (d) Stacked spectra of an adjacent resonance largely detuned from all Aux resonances.

$\kappa_A^2 \sim 0.03$. The FSR of the auxiliary resonator is 2.1 nm and $\kappa_C^2 \sim 0.21$, yielding a Q of ~ 23000 . To demonstrate the change of the linewidth of a single resonance at $\lambda_0 = 1542.97$ (indicated with an arrow in Fig.3(b)) in the Main resonator, we recorded the transmission spectra at different detunings $\Delta\lambda_{\text{aux}} = \lambda_{\text{Aux}} - \lambda_0$ between the target resonance and the closest auxiliary resonance at λ_{Aux} . We then define the normalized distance between the two resonances as $\Delta\lambda_{\text{aux}}/\gamma_{\text{aux}}$, where $\gamma_{\text{aux}} = 0.067$ nm is the linewidth of the Aux resonance. The wavelength of the Aux resonance is swept from $\Delta\lambda_{\text{aux}}/\gamma_{\text{aux}} = 5$ to $\Delta\lambda_{\text{aux}}/\gamma_{\text{aux}} \sim -2$ in small steps. The different spectra are shown stacked in Fig.4(a), while Fig.4(b) reports T calculated using Eq.(1), which shows a good agreement with the experimental results. From the stacked spectra in Fig.4(a) we extracted the extinction and the linewidth $\Delta\lambda$ of the target resonance. In Fig.4(c) it is shown the quantity $\lambda/\Delta\lambda$, which coincides with the Q-factor when the Aux is highly detuned from the target Main resonance, as the latter restores its natural Lorentzian shape. The simultaneous analysis of the extinction and of the linewidth allows us to assess how the effective coupling κ_{eff}^2 between the Main resonator and the bus-waveguide changes due to the phase imparted by the Aux resonator. When $\Delta\lambda_{\text{aux}}/\gamma_{\text{aux}} \sim 2.5$, the extinction is almost zero, and $\lambda/\Delta\lambda$ approaches the value of the intrinsic Q. In this configuration, the resonator is

totally under-coupled at λ_0 . This is also confirmed from the simulation of κ_{eff}^2 as a function of $\Delta\lambda_{\text{aux}}/\gamma_{\text{aux}}$ (inset in Fig.4(b)), where κ_{eff} reaches its minimum value at $\Delta\lambda_{\text{aux}}/\gamma_{\text{aux}} \sim 2.5$. At $\Delta\lambda_{\text{aux}}/\gamma_{\text{aux}} \sim 1.4$, the extinction is maximized (~ -10 dB) and $\lambda/\Delta\lambda$ is half the intrinsic Q. This implies that the resonance is critically coupled, meaning that $\kappa_{\text{eff}} = \kappa_{\text{cc}}$ at λ_0 , as shown in the inset of Fig.4(b). When $\Delta\lambda_{\text{aux}}/\gamma_{\text{aux}} \rightarrow 0$, we have that $\lambda/\Delta\lambda$ reaches the minimum value of 6.5×10^4 , with an extinction of -0.25 dB, indicating a highly over-coupled resonance which is consistent with the maximum in κ_{eff}^2 shown in the inset of Fig.4(b).

To summarize, by sweeping the Aux resonance across the target resonance of the Main, we can continuously control $\lambda/\Delta\lambda$ between 6.5×10^4 and $\sim 3 \times 10^6$, realizing all the coupling regimes described in Sec.II. To confirm that the control of the Q-factor is wavelength-selective, in Fig.4(c) we also report the linewidth of a resonance at $\lambda_n \sim 1544.6$ nm, which is largely detuned from all Aux resonances. As $\Delta\lambda_{\text{aux}}$ changes, the Q-factor remains mostly unperturbed. The stacked spectra around the resonance at λ_n are shown in Fig.4(d). The slight redshift of the resonance wavelength is caused by the thermal cross-talk between the micro-heater on top of the Aux resonator and the Main resonator.

IV. CONCLUSIONS

We proposed and experimentally validated an integrated photonic device consisting of a microresonator where the Q-factor of a single resonance can be selectively changed, leaving that of the other resonances unperturbed. This is accomplished by a resonant interferometric coupler, in which an auxiliary resonator allows us to change the interference condition in a very narrow-band spectral range. We theoretically investigated several configurations, in which one resonance of the Main resonator is tuned from being maximally over-coupled to be totally under-coupled, leaving the other resonances unchanged. We experimentally validated the working principle of the device on the silicon nitride platform. The fabricated device enables the selective switching of the quality factor of a target resonance from 6.5×10^4 to 3×10^6 . By adding more than one Aux resonator in the long arm of the MZI we could target different resonances and independently control them. Thus, our design is highly modular and scalable. Many applications that require the resonant

control of the light matter interaction in nonlinear and quantum optics could benefit from our structure. Examples include Q-switched lasers, wavelength-selective integrated parametric oscillators, entangled photon pair generation and photon pair sources with simultaneously high brightness heralding efficiency.

ACKNOWLEDGEMENTS

P.L.P. acknowledges funding from the HyperSpace project (project ID 101070168). D.B acknowledges the support of Italian MUR and the European Union - Next Generation EU through the PRIN project number F53D23000550006 - SIGNED. M.B., M.G and M.L. acknowledge the PNRR MUR project PE0000023-NQSTI. All the authors acknowledge the support of Xanadu Quantum Technology for providing the samples and the useful discussions.

-
- [1] Z. Qiang, W. Zhou, and R. A. Soref, Optical add-drop filters based on photonic crystal ring resonators, *Optics express* **15**, 1823 (2007).
- [2] Y. Huang and T. Zhang, An optical filter based on micro-ring resonator and bragg grating, in *AOPC 2020: Optoelectronics and Nanophotonics; and Quantum Information Technology*, Vol. 11564 (SPIE, 2020) pp. 24–27.
- [3] M. Mokhtari, Tunable optical filter design with ring resonator based sagnac loop, *Optik* **242**, 167068 (2021).
- [4] M. A. Selim and M. Anwar, Enhanced q-factor and effective length silicon photonics filter utilizing nested ring resonators, *Journal of Optics* **25**, 115801 (2023).
- [5] D. Lin, S. Shi, W. Cheng, P. Liu, M. Lu, T. Lin, G. Hu, B. Yun, and Y. Cui, A high performance silicon nitride optical delay line with good expansibility, *Journal of Lightwave Technology* **41**, 209 (2022).
- [6] W. Shan, L. Lu, X. Wang, G. Zhou, Y. Liu, J. Chen, and L. Zhou, Broadband continuously tunable microwave photonic delay line based on cascaded silicon microrings, *Optics Express* **29**, 3375 (2021).
- [7] P. Steglich, D. G. Rabus, C. Sada, M. Paul, M. G. Weller, C. Mai, and A. Mai, Silicon photonic micro-ring resonators for chemical and biological sensing: A tutorial, *IEEE sensors journal* **22**, 10089 (2021).
- [8] N. L. Kazanskiy, S. N. Khonina, and M. A. Butt, A review of photonic sensors based on ring resonator structures: Three widely used platforms and implications of sensing applications, *Micromachines* **14**, 1080 (2023).
- [9] M. Moradi, M. Mohammadi, S. Olyaei, and M. Seifouri, Design and simulation of a fast all-optical modulator based on photonic crystal using ring resonators, *Silicon* , 1 (2021).
- [10] D. E. Hagan, M. Ye, P. Wang, J. C. Cartledge, and A. P. Knights, High-speed performance of a tdfa-band micro-ring resonator modulator and detector, *Optics Express* **28**, 16845 (2020).
- [11] M. A. Foster, J. S. Levy, O. Kuzucu, K. Saha, M. Lipson, and A. L. Gaeta, Silicon-based monolithic optical frequency comb source, *Optics Express* **19**, 14233 (2011).
- [12] B. Shen, L. Chang, J. Liu, H. Wang, Q.-F. Yang, C. Xi, R. N. Wang, J. He, T. Liu, W. Xie, *et al.*, Integrated turnkey soliton microcombs, *Nature* **582**, 365 (2020).
- [13] T. J. Kippenberg, A. L. Gaeta, M. Lipson, and M. L. Gorodetsky, Dissipative kerr solitons in optical microresonators, *Science* **361**, eaan8083 (2018).
- [14] M. Kues, C. Reimer, P. Roztocky, L. R. Cortés, S. Sciara, B. Wetzel, Y. Zhang, A. Cino, S. T. Chu, B. E. Little, *et al.*, On-chip generation of high-dimensional entangled quantum states and their coherent control, *Nature* **546**, 622 (2017).
- [15] X. Lei, C. Wieschendorf, J. Firth, F. Ladouceur, A. Furbach, and L. Silvestri, Numerical modelling and optimization of actively q-switched waveguide lasers based on liquid crystal transducers, *Optics Express* **27**, 8777 (2019).
- [16] K. Shtyrkova, P. T. Callahan, N. Li, E. S. Magden, A. Ruocco, D. Vermeulen, F. X. Kärtner, M. R. Watts, and E. P. Ippen, Integrated cmos-compatible q-switched mode-locked lasers at 1900nm with an on-chip artificial saturable absorber, *Optics express* **27**, 3542 (2019).
- [17] S. A. Miller, Y. Okawachi, S. Ramelow, K. Luke, A. Dutt, A. Farsi, A. L. Gaeta, and M. Lipson, Tunable frequency combs based on dual microring resonators, *Optics express* **23**, 21527 (2015).
- [18] H. Shoman, H. Jayatilleka, A. H. Park, A. Mistry, N. A. Jaeger, S. Shekhar, and L. Chrostowski, Compact wavelength-and bandwidth-tunable microring modulator, *Optics express* **27**, 26661 (2019).
- [19] Y. Liu, A. R. Wichman, B. Isaac, J. Kalkavage, E. J. Adles, T. R. Clark, and J. Klamkin, Ultra-low-loss silicon nitride optical beamforming network for wideband wireless applications, *IEEE Journal of Selected Topics in*

- Quantum Electronics **24**, 1 (2018).
- [20] Y. Zhang, Q. Liu, C. Mei, D. Zeng, Q. Huang, and X. Zhang, Proposal and demonstration of a controllable q factor in directly coupled microring resonators for optical buffering applications, *Photonics Research* **9**, 2006 (2021).
- [21] J. K. Rakshit, K. E. Zoiros, and G. K. Bharti, Proposal for ultrafast all-optical pseudo random binary sequence generator using microring resonator-based switches, *Journal of computational Electronics* **20**, 353 (2021).
- [22] Z. Vernon, M. Menotti, C. Tison, J. Steidle, M. Fanto, P. Thomas, S. Preble, A. Smith, P. Alsing, M. Liscidini, *et al.*, Truly unentangled photon pairs without spectral filtering, *Optics letters* **42**, 3638 (2017).
- [23] N. Chen, Z. Wang, J. Wu, H. Li, S. He, Z. Fan, Y. Fan, X. Zhang, Q. Zhou, and J. Xu, Pushing photon-pair generation rate in microresonators by q factor manipulation, *Optics Letters* **48**, 5355 (2023).
- [24] B. M. BurrIDGE, I. I. Faruque, J. G. Rarity, and J. Barreto, Integrate and scale: A source of spectrally separable photon pairs, *arXiv preprint arXiv:2303.17258* (2023).
- [25] Y. H. Wen, O. Kuzucu, M. Fridman, A. L. Gaeta, L.-W. Luo, and M. Lipson, All-optical control of an individual resonance in a silicon microresonator, *Physical Review Letters* **108**, 223907 (2012).
- [26] Y. H. Wen, O. Kuzucu, T. Hou, M. Lipson, and A. L. Gaeta, All-optical switching of a single resonance in silicon ring resonators, *Optics letters* **36**, 1413 (2011).
- [27] T. Guo, S. Gao, H. Zeng, L. Tang, and C. Qiu, All-optical control of a single resonance in a graphene-on-silicon nanobeam cavity using thermo-optic effect, *Journal of Lightwave Technology* **39**, 4710 (2021).
- [28] L. Chen, N. Sherwood-Droz, and M. Lipson, Compact bandwidth-tunable microring resonators, *Optics letters* **32**, 3361 (2007).
- [29] S. Manipatruni, C. B. Poitras, Q. Xu, and M. Lipson, High-speed electro-optic control of the optical quality factor of a silicon microcavity, *Optics letters* **33**, 1644 (2008).
- [30] X. Xue, Y. Xuan, P.-H. Wang, Y. Liu, D. E. Leaird, M. Qi, and A. M. Weiner, Normal-dispersion microcombs enabled by controllable mode interactions, *Laser & Photonics Reviews* **9**, L23 (2015).
- [31] C. M. Gentry, G. T. Garcés, X. Zeng, and M. A. Popović, Tailoring of individual photon lifetimes as a degree of freedom in resonant quantum photonic sources, in *CLEO 2016: Conference on Lasers and Electro-Optics, JTu5A.17* (Optica Publishing Group, 2016).